Materials Science and Engineering A 527 (2010) 6224–6229

Contents lists available at ScienceDirect

Materials Science and Engineering A

journal homepage: www.elsevier.com/locate/msea

Analysis on shear deformation mechanism of metallic glass under confined bending test

J.X. Zhao [a], F.F. Wu [a,b], Z.F. Zhang [a,*]

[a] Shenyang National Laboratory for Materials Science, Institute of Metal Research, Chinese Academy of Sciences, 72 Wenhua Road, Shenyang 110016, China
[b] School of Materials Science and Engineering, Liaoning University of Technology, 169 Shiying Street, Jinzhou 121001, China

ARTICLE INFO

Article history:
Received 18 March 2010
Received in revised form 28 May 2010
Accepted 14 June 2010

Keywords:
Metallic glasses
Confined bending test
Plastic deformation
Shear bands

ABSTRACT

The shear deformation mechanism of Zr-based metallic glass under multiaxial loadings was systematically analyzed. By means of a confined bending test (CBT), some regular shear bands (SBs) initiated on the tension surface of the specimen and the metallic glass showed certain plastic deformation ability due to the stable propagation of SBs. Moreover, the angles between most of the SBs and the edges of the specimen were measured to be 55° approximately. In order to reveal the shear deformation mechanism under the CBT, a nonlinear contact analytical model based on the finite element method (FEM) was proposed. Furthermore, according to the stress results obtained by simulations, a stress analysis method was employed to establish the relationship between the SB angle and the shear deformation process. Finally, compared with the experimental results above, it was concluded that the stress gradient produced by CBT was the key factor which could stimulate certain plasticity. Additionally, the initiation and propagation of the SBs were stable due to the multiaxial stress state in specimen.

1. Introduction

Due to the several properties attractive in structural materials, such as high yield strength, high hardness, metallic glasses have received much attention by many investigators [1–6]. Under uniaxial tension, the metallic glass fails along individual shear band (SB) rapidly and displays little plasticity [7–9]. Furthermore, under uniaxial compression, the specimens often yield by the propagation of primary SB with low plasticity (about 1–2%) [9–14]. However, when the aspect ratio of the compressive specimen is smaller than 1, owing to the constraint of the pressure machine, the plentiful SBs result in a large plasticity enhancement, which is quite different from the situation with an aspect ratio of 2 under uniaxial compressive loadings [15–22]. Under bending loading, metallic glass also displays a strong size effect on the ductility when the specimen's dimension is below a critical value [23,24]. Additionally, employing the experimental approaches and theoretical analysis, the deformation mechanisms under bending tests were investigated [25–28]. Besides, small punch test (SPTs) was used to reveal the SBs disciplines under multiaxial loadings [29,30], the results demonstrated that the metallic glass could be controlled to create regular arranged fine multiple SBs with a large plastic strain (19.6%) [30]. All the above approaches indicate that metallic glass could display different shear deformation behaviors and the plasticity also shows great differences under uniaxial tension and compression, bending and multiaxial loadings, separately. Therefore, it is necessary to analyze the shear deformation mechanism of metallic glass under different loadings, especially multiaxial loadings. In the present study, based on the confined bending test (CBT), the initiation and propagation of SBs in a Zr-based metallic glass are investigated, the analytical results may be applied to understand and evaluate the plastic deformation behaviors of metallic glass under multiple loading conditions.

2. Experimental procedures

The Zr-based metallic glass alloy of $Zr_{52.5}Ni_{14.6}Al_{10}Cu_{17.9}Ti_5$ was prepared by arc-melting. The final ingots had a rectangular shape, with the dimensions of $60.0 \times 30.0 \times 3.0\,mm^3$. A confined bending test (CBT) technique was applied to measure the mechanical properties of the as-cast specimens, as illustrated in Fig. 1. The metallic glass samples were cut into several strips with the dimensions of $15.0 \times 3.0 \times 0.38\,mm^3$. The steel head was 1.5 mm in diameter. The CBT was carried out with an MTS810 testing machine at room temperature in air. All the tests were conducted using a constant crosshead rate of about $0.001\,mm\,s^{-1}$. After the CBT, all the specimens were observed with scanning electron microscope (SEM) to reveal the deformation and fracture features. Besides, a finite element method (FEM) with the commercial finite element software ANSYS was exploited for simulating the stress states in the cur-

* Corresponding author. Tel.: +86 24 23971043; fax: +86 24 23891320.
E-mail address: zhfzhang@imr.ac.cn (Z.F. Zhang).

0921-5093/$ – see front matter © 2010 Elsevier B.V. All rights reserved.
doi:10.1016/j.msea.2010.06.039

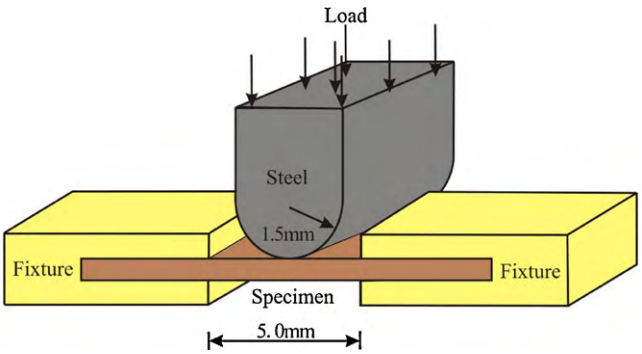

Fig. 1. Schematic illustration of the apparatus in the confined bending test (CBT).

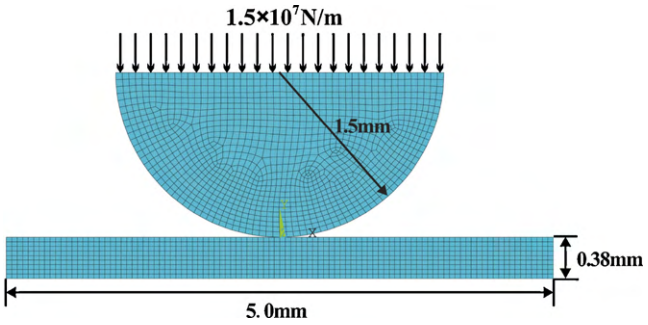

Fig. 3. Schematic illustration of the nonlinear contact analytical model by finite element simulation method.

rent experimental situations, which could display the numerical results of the nodes by dispersing the whole model into many finite elements [31].

3. Result and analysis

3.1. Observations on the formation of shear bands

As the SEM images shown in Fig. 2(a), the load F is applied on the specimen from the bottom to the top. Under the CBT, the metallic glass specimen is compressed into a bent strip [25,26], which shows certain plasticity unlike the situation under unixial tension or compression [3,9]. Wherein, many regular SBs display in symmetrical distribution on the tension surface. For further analysis, we marked two lines representing the different positions along two directions: L_1 stands for the length direction of the specimen, while L_2 represents the thickness direction of the sample. The lines L_1 and L2 intersect into one point, which is marked as *O*. Fig. 2(b) shows a magnified image on the region around the midpoint *O*. Obviously, plentiful SBs are formed around the midpoint symmetrically, meanwhile, the shear displacement in the upper surface is larger than that in the inside region. It implies that the SBs might expand from surface to inside, and yielding and shearing should occur in upper surface firstly [25,26]. Furthermore, as shown in Fig. 2(c) and (d), the separated SBs arrange in parallel with a shear angle of 55° approximately, these angle values are the same as the ones under the uniaxial tension test, strictly [8,9]. Therefore, all the above results need a further investigation on the formation of SBs under the CBT, which is beneficial to understanding of the plastic deformation behaviors of metallic glass under multiaxial loadings.

3.2. Finite element analysis on shear deformation

For bending tests, Conner et al. [25] have given a detailed theoretical analysis about the stress states. In order to obtain the quantitative numerical results perfectly, a finite element model (FEM) was applied to compute the stress states, as displayed in Fig. 3. The results show that the local results are more suitable for the multiaxial loadings, compared with the theoretical results [25]. In the FEM model, a plane stress analysis was built by the finite

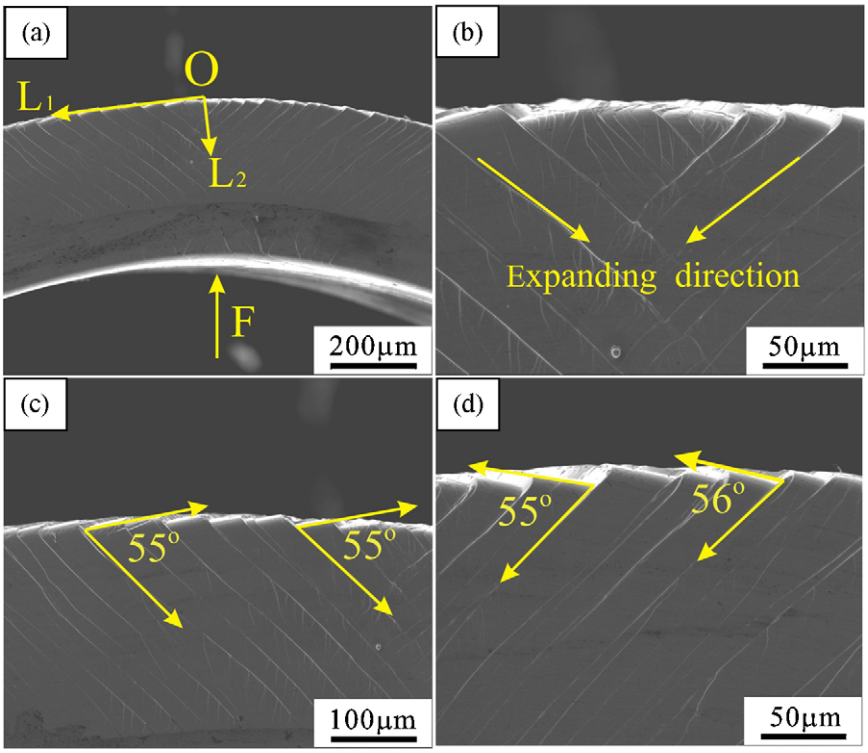

Fig. 2. (a) The photograph of $Zr_{52.5}Ni1_{4.6}Al_{10}Cu_{17.9}Ti_5$ metallic glass after experiment, (b) magnified image of the region around the midpoint O region; (c and d) magnified photographs of shear bands.

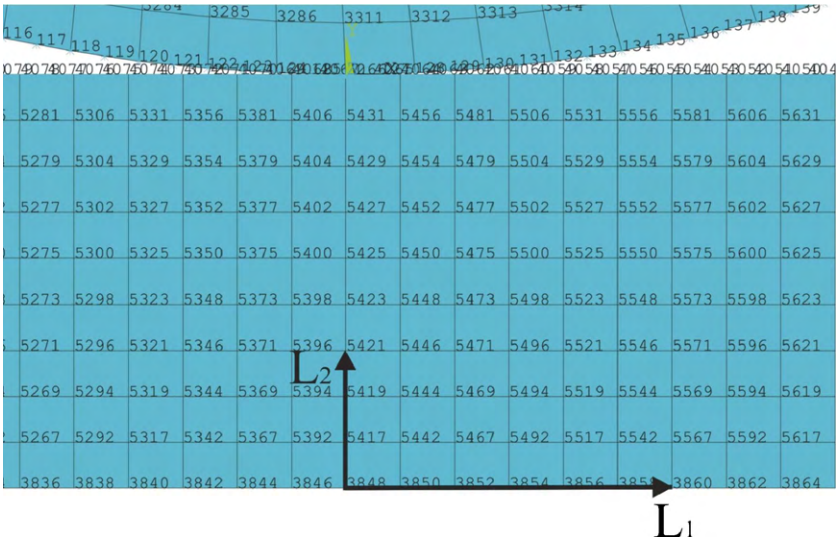

Fig. 4. Distribution of nodes in the simulated model.

element software while the dimensions of the model were accordant with the experimental data. A point-to-line nonlinear contact analytical model was used to simulate the CBT processes, a static analysis could describe the test reasonably, since the strain rate was slow enough and the metallic glass displayed zero plasticity under tension and plasticity [9]. In this model, a linear uniform pressure loading (1.5×10^7 N/m) was adopted to imitate the pressure head with a fixed boundary on the both ends of specimen model. The elastic modulus and Poisson's ratio of metallic glass are 97.8 GPa and 0.36 separately [9,32]. Because the pressure head in the test was made of rigid materials, the corresponding elastic modulus and Poisson's ratio could be confirmed as 210 GPa and 0.30, respectively [33]. Then, in terms of the above analysis, the schematic illustration of grid nodes constructed by the finite element software is displayed in Fig. 4. Here, L_1, L_2 and O represent the same meanings as those in Fig. 2(a), in order to compare the experimental data with the simulated results. The nodes along the line L_1 are 3848, 3850, 3852, 3854, 3856, 3860, where the calculated results could express the stress states along the length direction. Equally, the numerical results about the nodes marked as 3848, 5417, 5419, 5421 could reflect the stress conditions along the thickness direction L_2. Then, by the computer simulations, the mechanical informations of the nodes such as stress and strain could be gained.

3.3. Formation mechanism of shear bands

On the basis of the numerical results, the stress analysis method was proposed to study the formation mechanism of SBs in the CBT. As illustrated in Fig. 5, the biaxial stressed state unit [34] was displayed. Herein, the normal and shear stresses are marked as σ_x, σ_y and τ_{xy}. The dashed line stands for the random section and the angulation between this section and the x direction is θ, the corresponding normal and shear stresses are marked as σ_θ and τ_θ. Therefore, the relationship among σ_x, σ_y, τ_{xy} and σ_θ, τ_θ could be written as [34]:

$$\sigma_\theta = \frac{\sigma_x + \sigma_y}{2} + \frac{\sigma_x - \sigma_y}{2} \cos 2\theta - \tau_{xy} \sin 2\theta \quad (1)$$

$$\tau_\theta = \frac{\sigma_x - \sigma_y}{2} \sin 2\theta + \tau_{xy} \cos \theta \quad (2)$$

For metallic glasses, numerous experimental results indicate that the initiation of SBs in various metallic glasses is not only decided by the shear stress, but also influenced by the normal stress on the shear plane [3,9,12,35]. Hereby, if considering the effect of normal stress, the Mohr–Coulomb criterion [36,37] and the unified tensile fracture criterion [38] were separately used to analyze the formation mechanism of SBs under CBT. Firstly, for the nodes along L_1 and L_2, the stress values on random sections were attained by the simulations. Then, we calculated the maximal stress section by the Mohr–Coulomb criterion, as expressed below:

$$\tau \geq \tau_0 + \mu\sigma. \quad (3)$$

Here, τ and σ represent the shear and normal stresses on the random section in the biaxial stressed state unit [34], respectively. τ_0 is the critical shear stress while μ stands for the internal friction coefficient in the fracture process. For the $Zr_{52.5}Ni_{14.6}Al_{10}Cu_{17.9}Ti_5$ metallic glass, μ could be determined as 0.364 under tension loading [8,12]. Then, substituting Eqs. (1) and (2) to Eq. (3), the imaginary general shear stress τ_g^{MC} could be taken as:

$$\tau_g^{MC} = \tau_\theta + \mu \cdot \sigma_\theta \quad (4)$$

Deriving τ_g^{MC} by θ, $d\tau_g^{MC}/d\theta = 0$, we can obtain the mathematical condition when τ_g^{MC} reaches its maximal value τ_{max}:

$$\tan 2\theta = \frac{(\sigma_x - \sigma_y) - 2\mu\tau_{xy}}{2\tau_{xy} + \mu(\sigma_x + \sigma_y)} \quad (5)$$

Therefore, according to the numerical results of σ_x, σ_y, τ_{xy} acquired by the finite element simulations, combined with the above stress analysis, the valuable results of nodes along L_1 and L_2

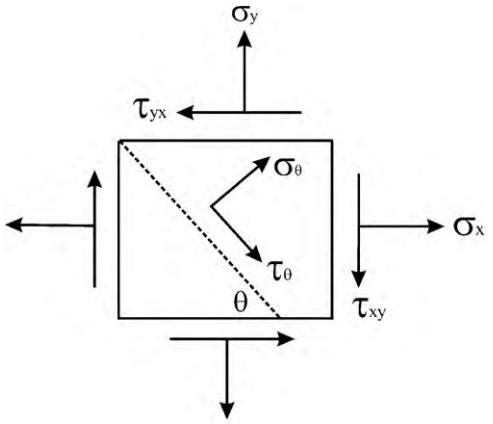

Fig. 5. Schematic illustration of biaxial stress state unit.

Table 1
The numerical results on nodes along L_1.

Node	σ_x (GPa)	σ_y (MPa)	τ_{xy} (MPa)	θ_{max}	τ_{max} (MPa)
3848	1.13	1.00	-7.18×10^{-5}	55°	804
3850	1.12	0.92	0.46	55°	798
3852	1.09	0.66	0.81	55°	777
3854	1.05	0.38	1.00	55°	748
3856	1.00	0.16	1.04	55°	713
3858	0.95	0.0265	0.99	55°	677
3860	0.90	−0.0322	0.91	55°	640

Table 2
The numerical results on nodes along L_2.

Node	σ_x (GPa)	σ_y (MPa)	τ_{xy} (MPa)	θ_{max}	τ_{max} (MPa)
3848	1.13	1.00	-7.18×10^{-5}	55°	804
5417	0.85	−5.7	−0.0227	55°	615
5419	0.61	−22.8	−0.0378	55°	442
5421	0.37	−47.8	−0.0508	55°	281

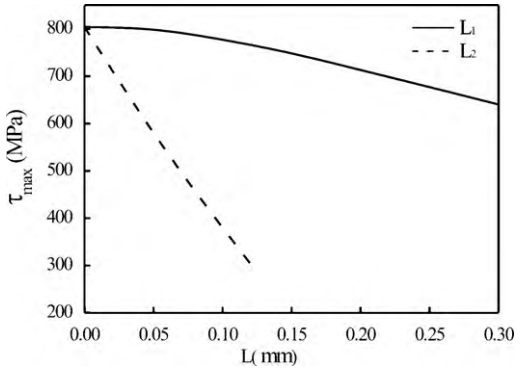

Fig. 6. Regular curves of τ_{max} with different nodes in L_1 and L_2.

were obtained, as showed in Tables 1 and 2. Here, θ_{max} expresses the angle from the maximal general shear stress (τ_g^{MC}) section to the x-direction. The results demonstrate that the shear angles are unified in the value of 55°, which are strictly identical with the experimental results in Fig. 2(c). For detailing the stress distributions along the L_1 and L_2 directions quantitatively, the values of τ_{max} for different nodes are displayed in Fig. 6. It could be found that τ_{max} fell down along the arrow direction (see Fig. 4), indicating that the stress in midpoint O had the maximum value and the metallic glass might yield from this region firstly. Contrast to the findings in Fig. 2(b), the midpoint region displays larger shear deformation than other districts. Moreover, along the arrow direction of L_1 and L_1, the shear deformation degree tends to decline (see Fig. 2(a)), indicating that the local simulated results could describe the stress states accurately. Moreover, compared with the two curves in Fig. 6, the values of τ_{max} in L_2 dropped faster than the results in L_1, suggesting that the regions along L_1 were more easily shaped than the districts along L_2. For this reason, in Fig. 2(a), the SBs started from the regions in L_1 and pointed to the L_2 districts. For further detailed description of the stress values on the random sections, the illustration of τ_g^{MC} with θ is expressed in Fig. 7 and the critical shear angles θ_{max} is 55° conformably.

Besides the Mohr–Coulomb criterion, the unified tensile fracture criterion [38] is utilized to assess the tensile shear fracture behavior of metallic glasses [12,35,38]. The related criterion equation could be expressed as:

$$\alpha^2 \cdot \sigma^2 + \tau^2 \geq \tau_0^2 \tag{6}$$

For simplifying the computational process, we marked $\tau_g^U = \sqrt{\alpha^2 \cdot \sigma^2 + \tau^2}$ as the general shear stress in biaxial stressed state unit [34]. Substituting Eqs. (1) and (2) to τ_g^U, the values of τ_g^U on the random sections computed by the unified tensile fracture criterion are shown in Fig. 8, and the values of θ_{max} are also equal to 55°, which are the same as the ones obtained by the Mohr–Coulomb criterion. In general, the stress states in CBT are quite different from the situations under tensile loadings. The stress gradient generated by the multiaxial loadings could result in the uneven fracture features illustrated in Fig. 2.

With the above two fracture criteria, the initiation and propagation of SBs in the CBT were evaluated by the stress analytical method, effectively. For the shear angle θ_{max}, the similar results had been obtained by the two criteria, indicating that the normal stress plays an important role in the formation of SBs under the multiple loadings. Therefore, it has potential interest to propose and verify the fracture criteria by changing the arrangement of normal and shear stresses on metallic glasses.

3.4. Comparison of shear deformation and plasticity

By contrast, under uniaxial tensile loadings [7–9], little plasticity was observed since the specimen had the uniform stress field and the SBs could expand rapidly till the material failed without any rotation of SBs. The similar phenomena had been found in other metallic glasses [39,40]. Moreover, different from the tensile properties slightly, the Zr-based metallic glass displayed little plasticity under compression tests [9,10], suggesting that the propagation of SBs may be confined by the limited compressive space during the fracture process, in spite of the uniform stress field distribution. Nevertheless, for CBT on metallic glasses [23–30], the stress gradient was created by the multiaxial loadings in the specimens

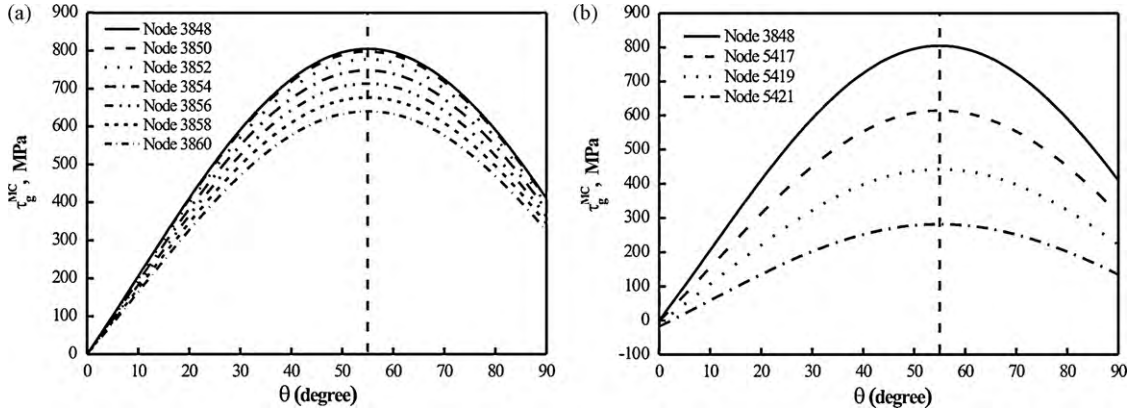

Fig. 7. Illustration of τ_g^{MC} with θ computed by the Mohr–Coulomb fracture criterion: (a) the curve about nodes in L_1; (b) the nodes in L_2.

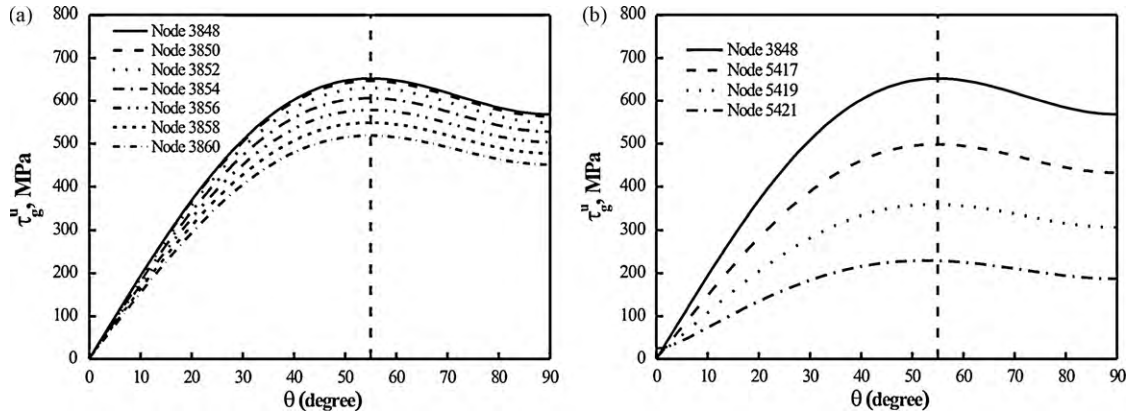

Fig. 8. Illustration of τ_g^U with θ obtained by the unified tensile fracture criterion: (a) the curve about nodes in L_1; (b) the nodes in L_2.

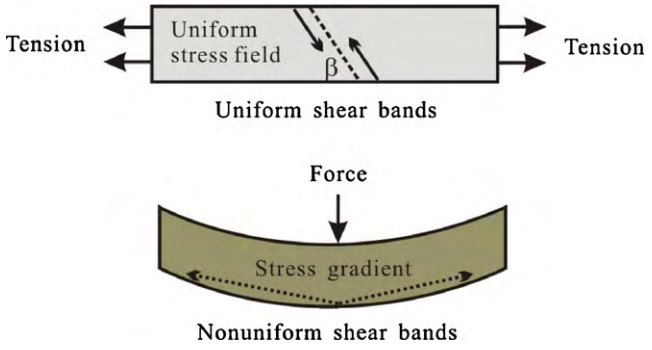

Fig. 9. Comparison of shear formation mechanism between the uniaxial tension and the confined bending test (CBT) on metallic glasses.

which can result in a considerable plasticity since the SBs could not spread along one SB due to the action of stress gradient. In brief, the plasticity of metallic glass depends on the difficulty level about the propagation of SBs. When the SBs are restricted or deflected, it is difficult for SBs to extend quickly, the obvious plasticity may be exploited reasonably.

4. Conclusions

A CBT was applied to investigate the formation mechanism of SBs in metallic glass. Interestingly, some regular SBs distributed on the tension surface of the specimen and the sample showed a larger plasticity than that under uniaxial tension loadings [7–9]. Used by the finite element method, a nonlinear contact model was used to analyze the stress distributions. According to the two common fracture criteria for metallic glass, the experimental results could be interpreted commendably. Additionally, for the purpose of understanding the formation mechanism of SBs in a visual way, the schematic illustrations under the uniaxial tension and the CBT loadings are given in Fig. 9. It is known that the metallic glass yields along one SB and displays little plasticity under tensile loadings [7–9], since the stress states in this situation are uniform without any stress gradient. However, under the CBT, stress gradient could be produced and the specimen should display an inhomogeneous stress distribution. Wherein, the shear stresses in some regions had reached the critical value, however, some other regions are still in the elastic stage. Then, the inhomogeneous SBs are difficult to be linked into one major SB so that the sample can not fracture quickly [3,9]. Instead, the whole specimen could display certain plasticity undoubtedly. As a result, on one hand, the plasticity of metallic glass could be improved by installing the stress gradient by mechanical or material methods, such as by changing the loading conditions [29,30], adding other phases into the primary materials [41] and processing one layer on the surface of metallic glass after shot peening [42]. On the other hand, by means of the CBT, the strength and plasticity of metallic glass under multiaxial loadings could be evaluated and new materials with high strength and plasticity may be developed in future.

Acknowledgements

The authors would like to thank Prof. Y.S. Yang for the technical assistance on the finite element software. This work was financially supported by the National Natural Science Foundation of China (NSFC) under Grant No. 50625103, 50871117 and 50890173, 50901038.

References

[1] H.S. Chen, Acta Metall. 22 (1974) 1505–1511.
[2] A. Inoue, Acta Mater. 48 (2000) 279–306.
[3] Z.F. Zhang, F.F. Wu, G. He, J. Eckert, J. Mater. Sci. Technol. 23 (2007) 747–767.
[4] C.A. Schuh, T.C. Hufnagel, U. Ramamurty, Acta Mater. 55 (2007) 4067–4109.
[5] W.H. Wang, C. Dong, C.H. Shek, Mater. Sci. Eng. R44 (2004) 45–89.
[6] P. Lowhaphandu, S.L. Montgomery, J.J. Lewandowski, Scripta Mater. 41 (1999) 19–24.
[7] C.T. Liu, L. Heatherly, D.S. Easton, C.A. Carmichael, J.H. Schneibel, C.H. Chen, J.L. Wright, M.H. Yoo, J.A. Horton, A. Inoue, Metall. Mater. Trans. A 29 (1998) 1811–1820.
[8] G. He, J. Lu, Z. Bian, D.J. Chen, G.L. Chen, G.C. Tu, G.J. Chen, Mater. Trans. JIM 42 (2001) 359–364.
[9] Z.F. Zhang, J. Eckert, J. Schultz, Metall. Mater. Trans. 35A (2004) 489–498.
[10] Z. Bian, T. Zhang, H. Kato, M. Hasegawa, A. Inoue, J. Mater. Res. 19 (2004) 1068–1076.
[11] W.J. Wright, R. Saha, W.D. Nix, Mater. Trans. 42 (2001) 642–649.
[12] Z.F. Zhang, J. Eckert, L. Schultz, Acta Mater. 51 (2003) 1167–1179.
[13] J. Shen, W.Z. Liang, J.F. Sun, Appl. Phys. Lett. 89 (2006) 121908.
[14] D.W. Xing, Y.J. Yang, J. Shen, J.F. Sun, Mater. Lett. 62 (2008) 44–46.
[15] C.A. Pampillo, H.S. Chen, Mater. Sci. Eng. A 13 (1974) 181–188.
[16] G.P. Sunny, V. Prakash, J.J. Lewandowski, Effects of annealing on dynamic behavior of a bulk metallic glass, in: Proceedings of the 2005 International Mechanical Engineering Conference and Exposition, New York, USA, 2005.
[17] Z.F. Zhang, H. Zhang, X.F. Pan, J. Das, J. Eckert, Philos. Mag. Lett. 85 (2005) 513–521.
[18] H. Bei, S. Xie, E.P. George, Phys. Rev. Lett. 96 (2006) 105503.
[19] G. Sunny, J. Lewandowski, V. Prakash, J. Mater. Res. 22 (2007) 389–401.
[20] F.F. Wu, Z.F. Zhang, S.X. Mao, J. Mater. Res. 22 (2007) 501–507.
[21] F.F. Wu, Z.F. Zhang, S.X. Mao, Acta Mater. 57 (2009) 257–266.
[22] Z. Han, W.F. Wu, Y. Li, Y.J. Wei, H.J. Gao, Acta Mater. 57 (2009) 1367–1372.
[23] A. Inoue, A. Katsuya, K. Amiya, T. Masumoto, Mater. Trans. JIM 36 (1995) 802–809.
[24] A. Katuya, A. Inoue, K. Amiya, Int. J. Rapid Solidif. 9 (1996) 137–158.
[25] R.D. Conner, W.L. Johnson, N.E. Paton, W.D. Nix, J. Appl. Phys. 94 (2003) 904–911.
[26] R.D. Conner, Y. Li, W.D. Nix, W.L. Johnson, Acta Mater. 52 (2004) 2429–2434.
[27] N.H. Tariq, B.A. Hasan, J.I. Akhter, M.A. Shaikh, J. Alloys. Compd. 479 (2009) 242–245.
[28] L.C. Zhang, F. Jiang, Y.L. Zhao, S.B. Pan, L. He, J. Sun, J. Mater. Res. 25 (2010) 283–291.

[29] F.F. Wu, Z.F. Zhang, F. Jiang, J. Sun, J. Shen, S.X. Mao, Appl. Phys. Lett. 90 (2007) 191909.
[30] F.F. Wu, Z.F. Zhang, J. Shen, S.X. Mao, Acta Mater. 56 (2008) 894–904.
[31] F.C. Wang, Z.H. Zhang, Analytical Theory of Finite Element for ANSYS 10.0 and Engineering Application, Publishing House of Electronics Industry, Beijing, 2006 (in Chinese).
[32] W.H. Wang, J. Appl. Phys. 99 (2006) 093506.
[33] H.H. Luo, G. Chen, P.C. Zhai, J. Wuhan Univ. Technol. (Chin. J.) 28 (2006) 23–26.
[34] H.C. Cai, X. Min, Material Mechanics, Xi'An Jiaotong University Press, Xi'An, 2004 (in Chinese).
[35] Z.F. Zhang, G. He, J. Eckert, L. Schultz, Phys. Rev. Lett. 91 (2003) 045505.
[36] B.I. Sandor, Strength of Materials, Prentice Hall, Englewood Cliffs, NJ, 1978.
[37] M.A. Mayers, K.K. Chawla, Mechanical Behavior of Materials, Prentice Hall, Upper Saddle River, NJ, 1999.
[38] Z.F. Zhang, J. Eckert, Phys. Rev. Lett. 94 (2005) 094301.
[39] A. Inoue, H.M. Kimura, T. Zhang, Mater. Sci. Eng. A 294 (2000) 727–735.
[40] X.S. Xiao, S.S. Fang, L. Xia, W.H. Li, Q. Hua, Y.D. Dong, J. Alloys Compd. 351 (2003) 324–328.
[41] D.C. Hofmann, J.Y. Suh, A. Wiest, G. Duan, M.L. Lind, M.D. Demetriou, W.L. Johnson, Nature 451 (2008) 1085–1090.
[42] Y. Zhang, W.H. Wang, A.L. Greer, Nat. Mater. 5 (2006) 857–860.